

Article

Adsorption of Phenols from Aqueous Solution with A pH-Sensitive Surfactant-Modified Bentonite

Xiangfen Cui ¹, Jingmei Liao ¹, Huaying Liu ^{2,*}, Wei Tang ¹, Cheng Tie ³, Senlin Tian ¹ and Yingjie Li ^{1,*}

¹ Faculty of Environmental Science and Engineering, Kunming University of Science and Technology, No.727, South Jingming Road, Chenggong District, Kunming 650500, China; cui1987rainny@163.com (X.C.); tiansenlin@outlook.com (S.T.)

² Faculty of Chemical Engineering, Kunming University of Science and Technology, No.727, South Jingming Road, Chenggong District, Kunming 650500, China

³ Yunnan Ecological and Environmental Monitoring Center, No.539, Huancheng West Road, Xishan District, Kunming 650034, China; m13759502508@163.com

* Correspondence: liuhuaying86@sina.com (H.L.); yjli@kust.edu.cn (Y.L.)

Abstract: The presence of organic pollutants in wastewater remains a prominent environmental concern due to the related ecological and health hazards. In response, this study employs an adsorptive methodology to address the removal of phenol and catechol, utilizing an organo-bentonite material modified with a pH-responsive switchable surfactant, dodecyldimethylamine oxide (C₁₂DAO). The synthesized organo-bentonite (C₁₂DAO-Bt) manifests commendable thermostability resulting from thermogravimetric analyses. The adsorption capacities of C₁₂DAO-Bt concerning phenol and catechol intensify with the augmentation of the C₁₂DAO/bentonite mass ratio. The utmost adsorption capacities of 150C₁₂DAO-Bt, deduced through a pseudo-second-order kinetic model, stand at 5.72 mg·g⁻¹ for phenol and 5.55 mg·g⁻¹ for catechol, respectively. Subject to modification by a pH-responsive surfactant, conditions leaning towards weakly acidic and neutral conditions (pH = 6~7) are conducive to the adsorption of phenolic compounds. Conversely, alkaline conditions (pH = 8~9) facilitate the dissociation of adsorbates from adsorbents. The augmentation of cationic strength within the examined scope incites the adsorption procedure while impeding the desorption efficacy. In the case of cationic species with comparable ionic strengths, Na⁺ exhibited a superior effect on the adsorption–desorption dynamics of phenol, while Ca²⁺ exerts a more pronounced effect on those of catechol. Moreover, even following five consecutive acid–base regulation cycles, C₁₂DAO-Bt retains a relatively high adsorption capacity and desorption efficacy, which underscores its exceptional regenerative capacity for removing phenolic compounds from wastewater.

Keywords: pH-responsive surfactants; organic bentonite; reversible adsorption; phenolic pollutants; wastewater



Citation: Cui, X.; Liao, J.; Liu, H.; Tang, W.; Tie, C.; Tian, S.; Li, Y. Adsorption of Phenols from Aqueous Solution with A pH-Sensitive Surfactant-Modified Bentonite. *Separations* **2023**, *10*, 523. <https://doi.org/10.3390/separations10100523>

Academic Editor: Marek Majdan

Received: 27 June 2023

Revised: 21 September 2023

Accepted: 22 September 2023

Published: 26 September 2023



Copyright: © 2023 by the authors. Licensee MDPI, Basel, Switzerland. This article is an open access article distributed under the terms and conditions of the Creative Commons Attribution (CC BY) license (<https://creativecommons.org/licenses/by/4.0/>).

1. Introduction

The discharge of organic wastewater from industrial activities has presented significant environmental challenges. Phenol, catechol, and their derivatives, known as phenolic compounds or phenols, are hydrocarbon-based pollutants with one or more hydroxyl groups (–OH) attached to an aromatic ring [1]. These compounds are moderately soluble in water [1] and commonly found in the wastewater of various industries, such as oil and gas, paint manufacturing, phenolic resin production, pulp and paper factories, and pharmaceutical industries [2,3]. Renowned for their elevated toxicity towards humans, animals, and aquatic ecosystems [4,5], phenolic compounds, particularly in the presence of chlorine, exhibit a propensity for forming carcinogenic chlorophenols. Due to their hazardous nature, regulatory bodies like the United States Environmental Protection Agency (USEPA) have classified numerous phenols, including phenol and catechol, as priority waterborne pollutants [6]. The USEPA has stipulated a maximum allowable phenol concentration of

0.006 mg·L⁻¹ for a ten-day exposure and 0.002 mg·L⁻¹ for lifetime exposure [7]. In addition to its similar toxic properties to phenol, catechol has been recognized to induce genotoxic effects, leading to mutations, DNA breakage, and chromosomal aberrations [8]. Herein, it is of utmost importance to remove these phenolic compounds from wastewater prior to their dissemination into aquatic ecosystems and soil matrices.

To counteract the ecological and health hazards of phenols, a range of technologies encompassing adsorption [9], extraction [10], chemical oxidation [3], distillation and evaporation [11], membrane separation [12], and biodegradation [5] have been developed for treating phenol-contaminated wastewater [7]. Among these, adsorption—which utilizes solid adsorbents such as activated carbon and ion exchange resins renowned for their remarkable adsorption capacities for phenols—has gained wide prominence [9,13]. However, their relatively high costs have limited extensive adoption. As a result, research endeavors have concentrated on the development of economical adsorbents like clay minerals, which possess substantial surface area and robust chemical stability [14]. Bentonite, among various clay minerals, emerges as a naturally abundant material endowed with the potential for enhanced adsorption capacity through the insertion of organic moieties into its inter-laminar spaces [15–17]. Nevertheless, the inherent hydrophilicity of raw bentonite restricts its efficacy in adsorbing organic pollutants, including phenols [18]. To surmount this limitation, surfactant modification has arisen as a promising strategy to enhance the adsorption efficiency of bentonite by modifying its surface chemistry and ameliorating its porous structure [9,18,19]. By introducing organic compounds, the resultant organo-bentonite exhibits enhanced pollutant removal capacities in aquatic environments [18,20,21].

A significant challenge that arises subsequent to the adsorption of organic pollutants using organic bentonite is the intricate liberation of adsorbed adsorbates due to the establishment of a thermodynamically stable hydrophobic organic phase within the material. Present treatment methods, including landfilling and desorption regeneration, encounter limitations. Landfilling is inherently impermanent and could potentially contribute to secondary pollution, while regeneration methods such as high-temperature heating, chemical oxidation, and biological approaches suffer from drawbacks like structural deterioration, high expenses, and protracted regeneration periods. In response, research efforts have been directed towards the development of environmentally responsive surfactants capable of altering micelle morphology and hydrophilicity–hydrophobicity equilibrium within a system through external stimuli such as electricity, light, heat, or acid [22,23]. Such surfactants have demonstrated reversible solubilization effects on hydrophobic organic pollutants. Building upon these findings, our prior study has successfully synthesized a novel electrochemically triggered, reversible organo-bentonite with switchable attributes based on ferrocene [24]. This unique surfactant exhibited excellent electrochemical reversibility and showcased an effective adsorption capacity for phenol.

Notably, the organic synthesis procedure of the electrochemical switch surfactant poses challenges in meeting the mass production demands of engineering applications. Conversely, the acquisition of pH-responsive surfactants is more straightforward and well established. pH-responsive surfactants can govern the morphological transformations of micelles by regulating the system's pH. An illustrative instance is the amphoteric surfactant of N, N-dimethyldodecylamine-N-oxide (C₁₂H₂₅N(CH₃)₂O, C₁₂DAO), which undergoes significant changes in self-assembly below its isoelectric point. Through pH adjustment, facile manipulation of micelle structure becomes feasible, enabling control over volume and hydrophilic–hydrophobic properties [25,26]. Nonetheless, the adsorption and regeneration abilities of pH-responsive surfactants in facilitating the reversible adsorption–desorption of organic pollutants remain unreported.

Leveraging this insight, we employed pH-responsive C₁₂DAO as a modifier to prepare an acid–base-regulated, switchable organic bentonite (C₁₂DAO-Bt) tailored for the removal of phenol and catechol from aqueous solution. We extensively investigated the effects of diverse conditions, including the C₁₂DAO/bentonite mass ratio, contact time, solution pH, ionic strength, and ionic species, on phenol and catechol adsorption, along with the

associated adsorption kinetics. Furthermore, we scrutinized the desorption efficacy and governing laws of C₁₂DAO-Bt under various experimental conditions. Additionally, the regenerative potential of C₁₂DAO-Bt was evaluated through a sequence of five consecutive acid–base-regulated cycles.

2. Materials and Methods

2.1. Chemicals

The Na-bentonite (purity 99%) utilized in this investigation was purchased from Tianjin Zhiyuan Chemical Reagent Co., Ltd. (Tianjin, China) boasting a cation exchange capacity (CEC) of 69 cmol·kg⁻¹. The C₁₂DAO (purity 30%) was procured from Shanghai Yien Chemical Technology Co., Ltd., Shanghai, China. Phenol (C₆H₅OH), sodium chloride (NaCl), potassium chloride (KCl), calcium chloride (CaCl₂), hydrochloric acid (HCl), and sodium hydroxide (NaOH) were all acquired from Shanghai Aladdin Biochemical Technology Co., Ltd., Shanghai, China. With the exception of Na-bentonite and C₁₂DAO, all other reagents were of analytical grade. Throughout the entirety of the experimental procedure, deionized water obtained using an ultrapure water machine (18.25 MΩ·cm, Nanjing Okai Environmental Technology Co., Ltd., Nanjing, China) was employed.

2.2. Reversibility of C₁₂DAO

C₁₂DAO stands as an exemplar of a pH-responsive surfactant, characterized by an extended hydrophobic tail juxtaposed with a small hydrophilic head group [27,28]. It incorporates a N-O bond, a pair of methyl groups (-CH₃), and the methylene groups (-CH₂) directly linked to nitrogen (-N-), contributing to the partial delocalization of positive charge [28]. Within an aqueous environment, the propensity for hydrophobic interactions drives the self-assembly of C₁₂DAO, culminating in the creation of cohesive micellar aggregates [27,28] with diverse morphologies, such as spheres, rods, discs, and vesicles [29]. These micellar entities play a pivotal role in dictating the rheological attributes of the resultant micellar solutions. Notably, solutions housing spherical micelles typically exhibit low viscosity, whereas those comprising cylindrical or worm-like micelles resemble polymer solutions, showcasing significant viscoelasticity [30,31]. The exceptional capability of worm-like micelles to enhance viscosity under flow conditions renders them compelling substitutes for conventional polymer-based fluids [31]. Thus, the measurement of relevant viscosity offers a macroscopic perspective for elucidating the reversible viscosity of C₁₂DAO. Furthermore, an investigation into surfactant micellar aggregates and their stability characterization can be conducted through Zeta potential detection, affording insights into transformative structural alterations [32]. To affirm the feasibility of effecting reversible modulation of C₁₂DAO via straightforward pH manipulation, a C₁₂DAO solution was prepared with a concentration of 64 mmol·L⁻¹. The solution's pH was systematically adjusted across the range of 2 to 10. Zeta potential measurements were executed employing a Zetasizer nano series Nano ZS 90 instrument (Malvern Panalytical Ltd., Malvern, UK). Furthermore, adhering to the stipulations outlined in GB/T 266-1988, viscosity measurements were undertaken at solution pH values of 9.5 and 6.4, with each process repeated thrice for every pH condition.

2.3. Synthesis of C₁₂DMAO-Bt

The Na-bentonite underwent a drying process at 50 °C for 3 h subsequent to being sifted through a 200-mesh sieve. Precisely 20 g of Na-bentonite was weighed and introduced into 100 mL of deionized water. Subsequently, a specific quantity of C₁₂DAO was added, and the amalgam was subjected to continuous agitation at 25 °C for 3 h. The resultant sample underwent suction filtration, followed by thorough washing with deionized water. This washing process was iterated 3~4 times until the absence of foam became evident. The modified bentonite (C₁₂DAO-Bt) acquired after the suction filtration and washing phases was dried for a span of 12 h within an electrothermal blast drying oven (101 type, Beijing Yongguangming Medical Instrument Co., Ltd., Beijing, China) maintained

at 40 °C. In this particular investigation, the synthesis of C₁₂DAO-Bt involved a varied range of C₁₂DAO/bentonite mass ratios, spanning 60% to 150%. The percentage values corresponded to the mass of C₁₂DAO added in relation to the cation exchange capacity (CEC) of the bentonite. The resulting bentonite specimens were designated as, for example, 60C₁₂DAO-Bt and 150C₁₂DAO-Bt. The calculation Formula (1) was utilized to ascertain the dosage of surfactant:

$$W = m \times CEC \times M \times a/b \quad (1)$$

where W denotes the surfactant mass, g; m represents the bentonite mass, g; CEC signifies the CEC content in bentonite, $\text{cmol} \cdot \text{kg}^{-1}$; M corresponds to the molar mass of the surfactant, $\text{g} \cdot \text{mol}^{-1}$; a signifies the modification ratio in percentage, %; b is the content of surfactant.

2.4. Structure Characterization of Raw-Bt and C₁₂DAO-Bt

The morphological attributes of raw and C₁₂DAO-modified adsorbents were comprehensively investigated using the Nova Nano SEM 450 scanning electron microscope (SEM). Drawing on previous research [33,34], the interlayer spacing of adsorbents was ascertained through X-ray diffraction (XRD) analysis conducted on a Rigaku Japan Ultima IV instrument. Employing a copper target and a wavelength (λ) of 0.15406 nm, the XRD analysis embraced a scanning speed of $2^\circ \cdot \text{min}^{-1}$ for comprehensive analysis. This XRD analysis facilitated the determination of the d_{001} value of adsorbents, thereby enabling an evaluation of alterations in interlayer dimensions within the organic montmorillonite framework across varying acid–base regulation proportions and distinct concentrations of surface-active agents [35]. An in-depth scrutiny of plausible variations in chemical structure was conducted via Fourier transform infrared spectroscopy (FTIR) to capture the infrared spectrum of adsorbents. Employing the powder conventional pressing mode, the FTIR analysis spanned a spectral range from 4000 cm^{-1} to 500 cm^{-1} . To gain insights into the thermal stability and composition of adsorbents, a meticulous thermogravimetric analysis (TGA) was executed using a PYRIS diamond instrument in a nitrogen environment with a heating rate of $10 \text{ }^\circ\text{C} \cdot \text{min}^{-1}$. With this context, TGA furnishes vital insights into the behavior of C₁₂DAO-Bt across diverse temperature gradients, thus offering valuable discernment [36].

2.5. Adsorption–Desorption of Phenols onto C₁₂DAO-Bt

Throughout this study, the experimental procedures were conducted at a controlled temperature of $25 \text{ }^\circ\text{C} \pm 2 \text{ }^\circ\text{C}$, and a constant agitation speed of 150 rpm was maintained over a duration of 4 h. In each experimental iteration, a solution volume of 20 mL containing phenol and catechol was employed alongside 2 g of the adsorbents under diverse factorial conditions, including C₁₂DAO/bentonite mass ratios, contact time, solution pH, ionic strength, and ionic species. Upon attaining adsorption equilibrium, a centrifugation step was carried out for 10 min using a high-speed cryogenic centrifuge operating at 3000 rpm. Subsequently, the supernatant was subjected to filtration through a membrane with a pore size of $0.45 \text{ }\mu\text{m}$. The resultant filtrate was reserved for subsequent analytical measurements. The quantification of phenol and catechol concentrations in the solutions was accomplished utilizing a UV-visible spectrophotometer (Thermo Evolution 201, Thermo Fisher Scientific, Waltham, MA, USA) at λ of 270 nm and 275 nm, respectively. The concentrations of both phenol and catechol displayed a linear correlation with the intensity of absorbance signals ($R^2 > 0.999$).

The equilibrium adsorption capacity (q_e) of adsorbate was calculated based on the difference between the initial and equilibrium concentrations in the supernatant [36], as illustrated by Equation (2).

$$q_e = (C_0 - C_e) \times \frac{V}{m} \quad (2)$$

where q_e represents the equilibrium adsorption capacity of adsorbates onto bentonite adsorbents ($\text{mg} \cdot \text{g}^{-1}$), and C_0 and C_e denote the initial and equilibrium concentration of

adsorbates in the solution ($\text{mg}\cdot\text{L}^{-1}$). V represents the volume of the aqueous solution (L), and m stands for the used adsorbent's mass (g).

The desorption behavior of adsorbates from the adsorbents was promptly explored upon achieving adsorption equilibrium. Following the removal of the supernatant, the residual sample was dried at $40\text{ }^\circ\text{C}$ until a constant weight was attained over a 12 h period. The resultant sample was reconstituted with 20 mL of deionized water, and the solution's pH was meticulously adjusted to fall within the controlled range of 8.5 to 10. Subsequently, the ensuing mixture underwent controlled agitation at a consistent temperature of $25\text{ }^\circ\text{C} \pm 2\text{ }^\circ\text{C}$ and a constant oscillation speed of 150 rpm for a period of 2 h. Upon attaining desorption equilibrium, the solution was subjected to centrifugation for 10 min at 3000 rpm using a high-speed cryogenic centrifuge. The resulting supernatant was then filtered through a $0.45\text{ }\mu\text{m}$ membrane, and the absorbance of adsorbates was assessed using the previously mentioned approach. The equilibrium concentration and desorption efficiency of the adsorbates in the supernatant were determined based on the post-desorption concentration alterations. The desorption rate was computed utilizing the specific Equation (3):

$$R = \frac{C}{(C_0 - C_e)} \times 100\% \tag{3}$$

where R represents the desorption rate (%), C signifies the adsorbate's concentration in the solution at desorption equilibrium ($\text{mg}\cdot\text{L}^{-1}$), and C_0 and C_e denote the initial concentration and equilibrium concentration of adsorbates in the solution during the adsorption process ($\text{mg}\cdot\text{L}^{-1}$), respectively.

3. Results and Discussion

3.1. pH-Responsive Zeta Potential and Viscosity of the C_{12} DAO System

Figure 1a portrays the Zeta potential profile of the C_{12} DAO system spanning the entire examined pH spectrum. Below pH 7, the C_{12} DAO system exhibits a positive Zeta potential, signifying the presence of predominantly positive charge within this pH range arising from cationic micelles. Evidently, the positive Zeta potential surpassed 30 mV within a pH interval of 6 to 7. Conversely, the system displays negative Zeta potential values under alkaline conditions. These observations align harmoniously with earlier studies [28,37] that established the positively charged nature of micellized C_{12} DAO molecules at low pH levels. In weakly acidic and neutral conditions, these molecules coexisted as mixed micelles in a zwitterionic and deprotonated configuration.

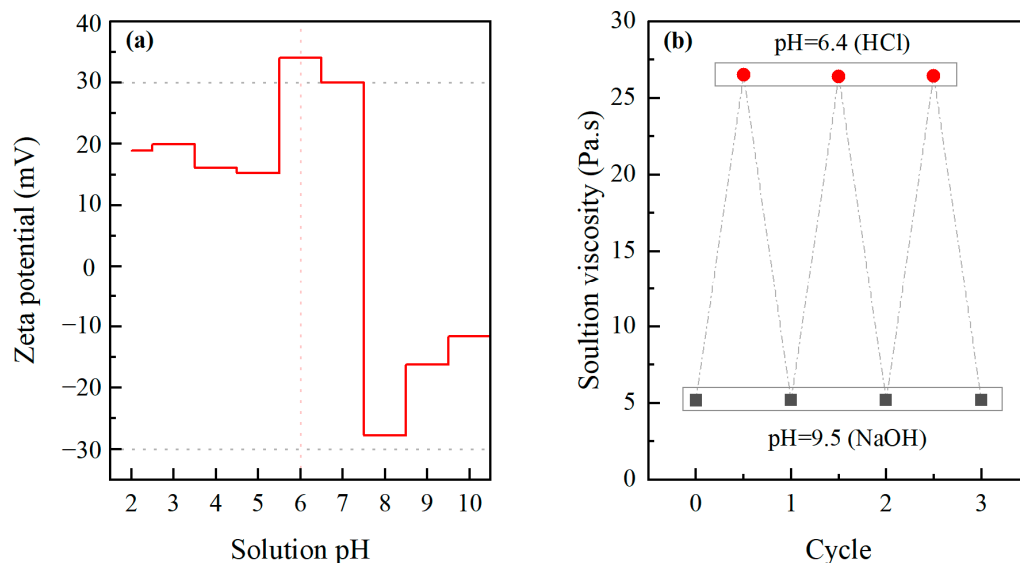


Figure 1. pH-responsive changes in (a) Zeta potential and (b) solution viscosity of C_{12} DAO system.

To delve deeper into the verification of C₁₂DAO’s acid–base switchable attributes, the solution viscosity was gauged across three consecutive acid–base regulation cycles through the adjustment of the pH to 6.4 and 9.5 via HCl and NaOH, respectively. As illustrated in Figure 1b, the solution’s viscosities were recorded as 5.2 Pa·s at pH 9.5 and 25.3 Pa·s at pH 6.4, respectively. These findings provide compelling evidence that C₁₂DAO undergoes a reversible structural transition in response to pH change, effectively showcasing its characteristic behavior as a reversibly switchable surfactant.

3.2. Characterizations of Adsorbents before Adsorption

Figure 2 provides SEM images of both raw and C₁₂DAO-modified bentonites. The SEM image of raw-Bt (Figure 2a) reveals a relatively compact and stratified surface structure with a plate-like morphology. In contrast, the SEM images of 100C₁₂DAO-Bt (Figure 2b) and 150C₁₂DAO-Bt (Figure 2c) display a looser surface with subtle curvature and an increased presence of protruding particles. This noticeable alteration can be attributed to the infiltration of C₁₂DAO within the bentonite layers, consequently augmenting the spacing between these layers.

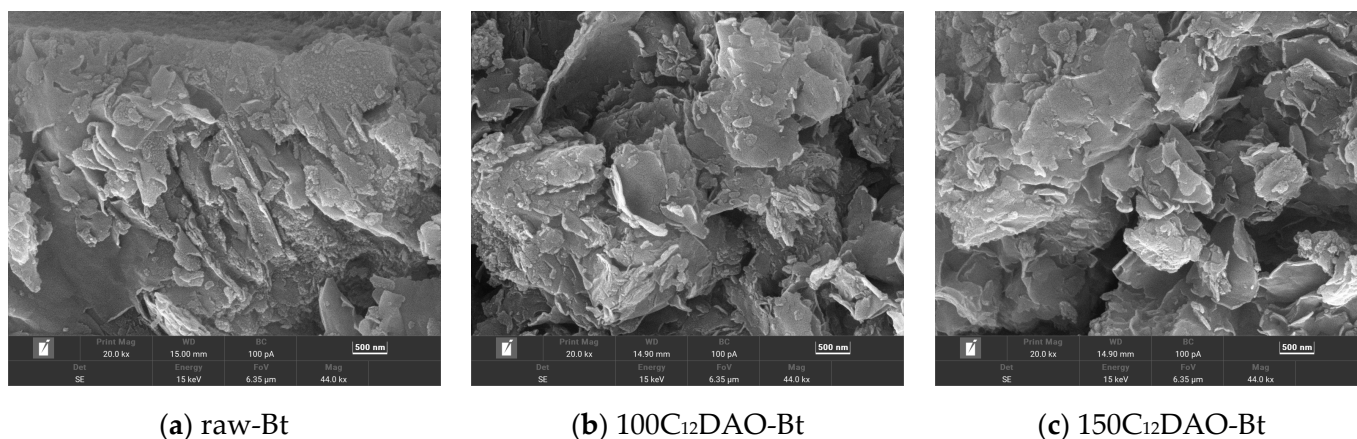


Figure 2. SEM images of adsorbents.

Figure 3a illustrates the XRD spectra of both raw-Bt and C₁₂DAO-Bt. The XRD spectra exhibit essentially consistent peak shapes between the raw and C₁₂DAO-modified adsorbents, with minimal observable variations. This observation implies that the modification process has not disrupted the inherent interlayered structure of the bentonites [36]. Nevertheless, the observed shifts in the position of the plane (001) diffraction peaks provide additional confirmation of alterations in the layer spacing [38]. Employing Bragg’s law ($2d \sin \theta = n\lambda$), the diffraction peak of raw-Bt was identified at 5.67°, corresponding to a d₀₀₁ value of 1.51 nm. In contrast, the diffraction peaks of 60C₁₂DAO-Bt, 80C₁₂DAO-Bt, 100C₁₂DAO-Bt, and 150C₁₂DAO-Bt were detected at 5.32°, 5.27°, 5.14°, and 5.11°, resulting in layer spacings of 1.61 nm, 1.62 nm, 1.67 nm, and 1.68 nm, respectively. Evidently, the layer spacing of C₁₂DAO-Bt exhibited a discernible increase with higher surfactant dosage. These findings provide evidence of the successful intercalation of C₁₂DAO within the bentonite interlayer [35] and the concurrent expansion of layer spacing [36]. However, the marginal difference (1.68 nm – 1.67 nm = 0.01 nm) observed in the interlayer spacing measurements between 150C₁₂DAO-Bt and 100C₁₂DAO-Bt serves as an indication that an excessive amount of surfactant did not infiltrate the bentonite interlayer.

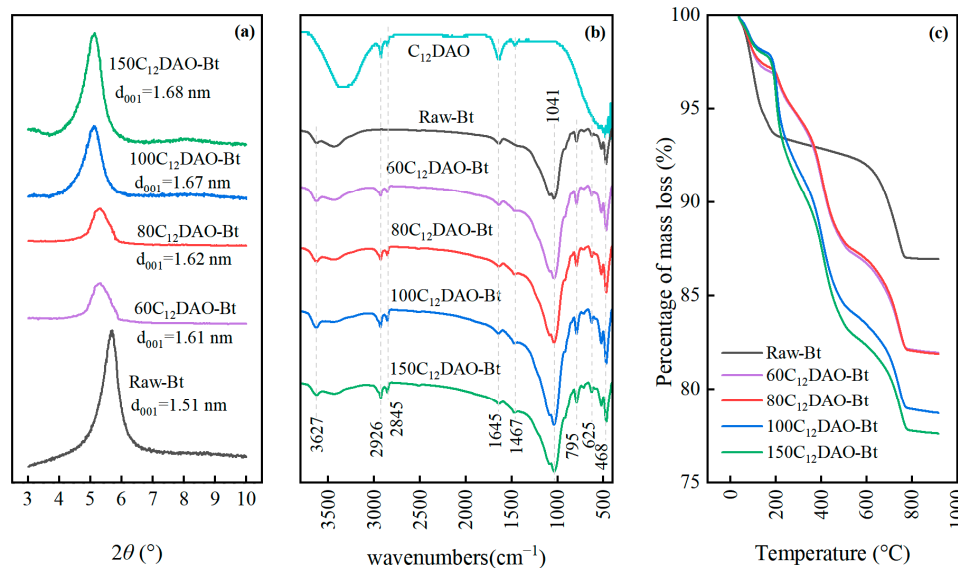


Figure 3. XRD spectra (a), FTIR spectra (b), and TG curves (c) of raw and C₁₂DAO-modified bentonite.

Figure 3b presents the FTIR spectra of C₁₂DAO and adsorbents before and after adsorption. Consistent with earlier studies [36,39], the characteristic peaks of the bentonite composites are evident at specific wavenumbers, including 3627 cm⁻¹ attributed to Al-OH and Si-OH stretching vibrations, 3436 cm⁻¹ associated with O-H and N-H stretching vibrations, 1645 cm⁻¹ indicative of H-O-H bending vibration, 1041 cm⁻¹ linked to Si-O stretching, 795 cm⁻¹ pertaining to Al-OH vibration, 625 cm⁻¹ corresponding to Al-O stretching, and 523 cm⁻¹ and 468 cm⁻¹ related to Si-O bending. A comparative analysis with raw-Bt reveals noticeable shifts in the C₁₂DAO-Bt spectra, particularly the antisymmetric and symmetric CH₂ stretching peaks at 2924 cm⁻¹ and 2845 cm⁻¹ [35,40] and the CH₂ bending vibration at 1467 cm⁻¹. Importantly, it becomes evident that C₁₂DAO loading allows observation of the shifts of symmetric and antisymmetric CH₂ stretching vibrations (Figure 4a). These findings imply the presence of an ordered or all-trans configuration of the alkyl chains on C₁₂DAO-Bt, augmenting van der Waals interactions between the alkyl chains and subsequently adsorbed substances [41]. Concurrently, the peak at 1467 cm⁻¹ arises from C-H vibrations [42]. Notably, the FTIR spectra of C₁₂DAO-Bt showcase an amplified peak at 3436 cm⁻¹ compared to raw-Bt, indicating hydrogen bond formation between the O-H group (3347 cm⁻¹) [43] of C₁₂DAO and the O-H group in the bentonite composites [36]. These findings strongly support that van der Waals interactions between the alkyl chains and adsorbate are reinforced with an increased loading of C₁₂DAO, but the incorporation of C₁₂DAO does not disrupt the fundamental skeletal structure of bentonites.

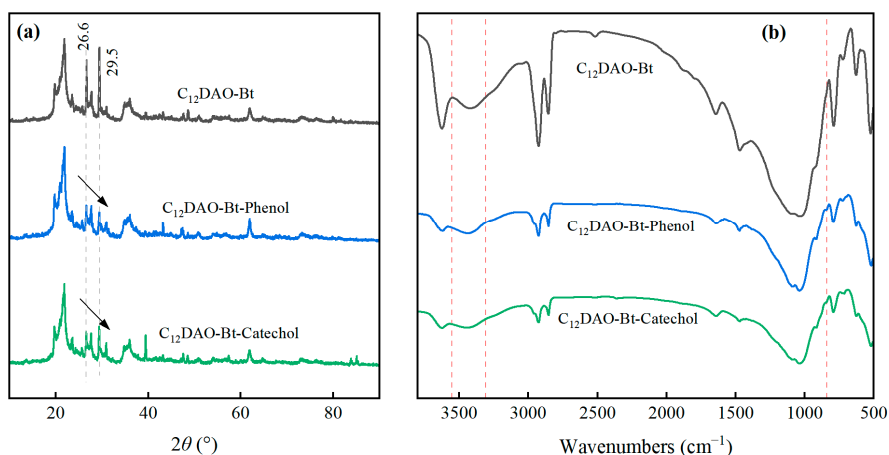


Figure 4. XRD spectra (a) and FTIR spectra (b) of 100C₁₂DAO-Bt after adsorption.

Figure 3c showcases the TGA curves depicting the thermal stability of both raw-Bt and C₁₂DAO-Bt. TGA curves offer insights into changes in adsorbent mass with elevating temperature. Evidently, the thermal degradation of raw-Bt is characterized by three distinct phases of mass loss. In the initial stage (37 °C~200 °C), a cumulative mass loss of 6.3% is observed, attributed to the desorption of physically absorbed H₂O within the raw-Bt matrix [44]. Subsequently, a minor mass loss stage (200~500 °C) is followed by a more substantial phase (500~767 °C), resulting in a mass loss of 12.87%. This significant weight reduction can be linked to the dehydroxylation of structural H₂O in raw-Bt, which leads to structural collapse and the loss of adsorption properties [44]. During the initial phase, the cumulative mass losses for 60C₁₂DAO-Bt, 80C₁₂DAO-Bt, 100C₁₂DAO-Bt, and 150C₁₂DAO-Bt were measured as 3.12%, 3.24%, 3.48%, and 4.17%, respectively—figures lower than those observed for raw-Bt. Within the temperature range of 200 °C to 500 °C, each variant of C₁₂DAO-Bt experiences more pronounced mass losses due to the partial decomposition of C₁₂DAO into CO₂, CO, and H₂O [36]. The observed mass loss trends of C₁₂DAO-Bt at each heating stage align with commonly noted mass loss patterns in conventional organic bentonite systems [33,36]. Given the significant overlap in TGA curves between 60C₁₂DAO-Bt and 80C₁₂DAO-Bt, three C₁₂DAO-modified bentonites were selected for further experimentation, excluding 80C₁₂DAO-Bt.

3.3. Characterizations of Adsorbents after Adsorption

Figure 4a presents XRD spectroscopy results for the 100C₁₂DAO-Bt sample both before and after the adsorption of phenol and catechol. Evidently, the fundamental structural integrity of adsorbent remains unaltered during the adsorption process. However, at 2θ values of 26.6° and 29.5°, there is a notable decrease in peak intensity after adsorption. This reduction can be attributed to the adsorption of phenol and catechol, which masks the crystal facets of the soil sample, leading to a decrease in exposed crystal facets. Figure 4b illustrates the FTIR spectra of 100C₁₂DAO-Bt before and after phenol and catechol adsorption. There was no observed shift in peaks assigned to 100C₁₂DAO-Bt during adsorption. However, its widened peak bands at 3300 and 3600 cm⁻¹ indicate the existence of the O–H group due to phenol adsorption. In addition, a new peak near 840 cm⁻¹ was observed in 100C₁₂DAO-Bt after both phenol and catechol adsorption.

3.4. Adsorption Studies

3.4.1. Effect of C₁₂DAO/Bentonite Ratios and Isothermal Fitting

In this investigation, the impact of different C₁₂DAO/bentonite mass ratios on the adsorption capacities of C₁₂DAO-Bt concerning both phenol and catechol was examined. Alongside the conditions outlined in Section 2.5, the experimental setup encompassed initial adsorbate concentrations set at 120 mg·L⁻¹ and a solution pH range spanning from 6.0~6.5. Among the test samples, 60C₁₂DAO-Bt, 100C₁₂DAO-Bt, and 150C₁₂DAO-Bt were chosen for batch adsorption, while raw-Bt served as the control. The outcomes of these experiments are illustrated in Figure 5a,b.

As shown in Figure 5a,b, the adsorption capacities of C₁₂DAO-Bt concerning both phenol and catechol at various C₁₂DAO/bentonite mass ratios surpassed that of raw-Bt. Moreover, the adsorption capacities of both these phenols displayed an upward trend with increasing C₁₂DAO dosage. These findings suggest a positive correlation between the adsorption capacity of C₁₂DAO-Bt and the dosage of C₁₂DAO. This observation underscores the role of the CEC in the adsorbents' performance for the removal of phenols.

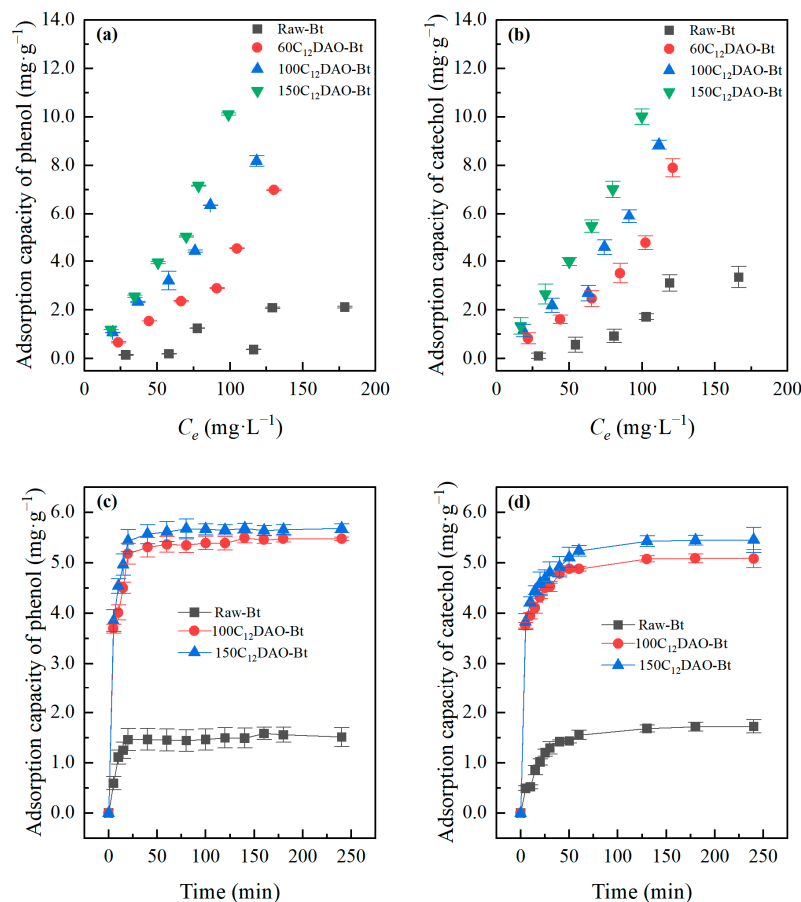


Figure 5. Effects of C₁₂DAO/bentonite mass ratios and contact time on adsorption capacity of phenol (a,c) and catechol (b,d).

Empirically, partitioning stands out as a pivotal mode of interaction between organic compounds and clays that have been modified through elongated carbon chain surfactants [45,46]. This mechanism signifies the solubilization of compounds within the organophilic matrix of the organo-clay. It is typically described through the lens of a partitioning coefficient, characterized by a linear isotherm, non-competitive sorption, and a notably restrained solute uptake [46]. The isothermal characteristic can be fitted using a linear model, as represented by Equation (4):

$$Q = K_d \times C_e \tag{4}$$

where Q is the mass of adsorbates onto adsorbents, $\text{mg}\cdot\text{g}^{-1}$, K_d represents the adsorption coefficient, and C_e denotes the equilibrium concentration of adsorbates in solution, $\text{mg}\cdot\text{L}^{-1}$. The adsorption efficiency of C₁₂DAO-Bt for phenol and catechol can be described through the carbon-normalized partition coefficient (K_{oc}), which can be calculated using Equation (5):

$$K_{oc} = K_d \times f_{oc} \tag{5}$$

where f_{oc} represents the mass of organic carbon content, $\text{g}\cdot\text{kg}^{-1}$. The parameters of the linear adsorption model and the resulting K_{oc} values for phenol and catechol on C₁₂DAO-Bt are summarized in Table 1.

Table 1. Parameters of linear isothermal model and carbon-normalized partition coefficient.

Phenolic Pollutants	Adsorbent	R ²	K _d	K _{oc}
Phenol	Raw-Bt	0.6331	0.0135	
	60C ₁₂ DAO-Bt	0.9152	0.0551	0.0001
	100C ₁₂ DAO-Bt	0.9715	0.0729	0.0009
	150C ₁₂ DAO-Bt	0.9550	0.1064	0.0012
Catechol	Raw-Bt	0.8686	0.3023	
	60C ₁₂ DAO-Bt	0.9786	0.4781	0.0044
	100C ₁₂ DAO-Bt	0.9114	0.6301	0.0082
	150C ₁₂ DAO-Bt	0.9950	0.8894	0.0105

As illustrated in Table 1, the adsorption behavior of both phenol and catechol by C₁₂DAO-Bt reveals a favorable linear correlation in comparison to the raw-Bt. The substantial linear correlation coefficient (R²) higher than 0.90 affirms the presence of partition-driven adsorption of phenol and catechol onto C₁₂DAO-Bt. Furthermore, the K_{oc} values exhibit a noticeable upsurge with an elevation of the C₁₂DAO/bentonite mass ratio. This noteworthy trend harmonizes seamlessly with the experimental observations delineated in Figure 4.

3.4.2. Effect of Contact Time and Kinetic Fitting

The impact of contact time on the adsorption capacities of C₁₂DAO-Bt for both phenol and catechol was examined in this study. Fourteen (5, 10, 15, 20, 25, 30, 35, 40, 50, 60, 80, 100, 120, 140, 160, 180, and 240 min) and thirteen (5, 10, 15, 20, 25, 30, 35, 40, 50, 60, 130, 180, and 240 min) temporal gradients were chosen to span from 0 to 240 min for batch adsorption of phenol and catechol. Adsorbents of 100C₁₂DAO-Bt and 150C₁₂DAO-Bt were selected as test samples, while raw-Bt served as the control. The results are presented in Figure 5c,d.

During the initial 50 min period, a swift and notable adsorption of both phenol (Figure 5c) and catechol (Figure 5d) onto C₁₂DAO-Bt was observed. This phenomenon can be ascribed to the notably high initial adsorbate concentrations, which expedited their rapid interaction with adsorbents. Furthermore, the abundance of active sites on the adsorbents’ surfaces significantly contributed to the heightened adsorption rate and augmented adsorption capacity during this initial phase. However, as the adsorption process extended beyond the initial 50 min, the solute concentration within the solution progressively declined, leading to a concomitant decrease in accessible active adsorption sites on C₁₂DAO-Bt. As a result, the adsorption rate gradually decelerated. It is noteworthy that during this stage, the adsorption capacity of C₁₂DAO-Bt for catechol surpassed that for phenol. After approximately 240 min, the adsorption sites on the C₁₂DAO-Bt reached a state of saturation, establishing adsorption equilibrium. The equilibrium adsorption capacities of 100C₁₂DAO-Bt and 150C₁₂MAO-Bt for phenol were determined to be 5.47 mg·g⁻¹ and 5.68 mg·g⁻¹, whereas the corresponding values for catechol were found to be 5.08 mg·g⁻¹ and 5.45 mg·g⁻¹.

To understand the adsorption process in depth, the kinetic data of adsorption were simulated by the pseudo-first-order kinetic model, pseudo-second-order kinetic model, and intraparticle diffusion model [36,47], as outlined in Equations (6)–(8).

$$\ln(q_e - q_t) = \ln q_e - k_1 t \tag{6}$$

$$\frac{1}{q_t} = \frac{1}{k_2 q_e^2} + \frac{t}{q_e} \tag{7}$$

$$q_t = k_{id} \times t^{1/2} + c \tag{8}$$

where q_t and q_e represent the adsorption mass (mg·g⁻¹) of solutes at time t and equilibrium, respectively. t (min) denotes adsorption time. k₁ (min⁻¹) and k₂ (g·mg⁻¹·min⁻¹)

correspond to the rate constant of the pseudo-first-order and second-order kinetic models; k_{id} ($\text{mg}\cdot\text{g}\cdot\text{min}^{1/2}$) is the intraparticle diffusion model constant representing the thickness of the boundary layer. The modelled parameters are summarized in Table 2.

Table 2. Parameters of the adsorption kinetic models of phenol and catechol adsorbed onto C12DAO-Bt.

Raw-Bt	Phenol		Catechol	
	100C12DAO-Bt	150C12DAO-Bt	100C12DAO-Bt	150C12DAO-Bt
Pseudo-first-order model				
k_1 (min^{-1})	0.024	0.038	0.024	0.038
q_e ($\text{mg}\cdot\text{g}^{-1}$)	1.05	0.79	0.20	2.22
R^2	0.751	0.694	0.822	0.942
Pseudo-second-order model				
K_2 ($\text{g}\cdot\text{mg}^{-1}\cdot\text{min}^{-1}$)	0.070	0.104	0.059	0.048
q_e ($\text{mg}\cdot\text{g}^{-1}$)	5.54	5.72	5.17	5.55
R^2	0.999	0.999	0.999	1.000
Intraparticle diffusion model				
$K_{id,1}$ ($\text{g}\cdot\text{mg}^{-1}\cdot\text{min}^{1/2}$)	0.489	0.698	0.256	0.383
c_1 ($\text{mg}\cdot\text{g}^{-1}$)	2.558	2.299	3.159	2.988
R^2	0.962	0.998	0.983	0.993
$K_{id,2}$ ($\text{g}\cdot\text{mg}^{-1}\cdot\text{min}^{1/2}$)	0.034	0.019	0.066	0.195
c_2 ($\text{mg}\cdot\text{g}^{-1}$)	5.057	5.468	4.382	3.714
R^2	0.869	0.751	0.785	0.995
$K_{id,3}$ ($\text{g}\cdot\text{mg}^{-1}\cdot\text{min}^{1/2}$)	0.005	0.015	0.002	0.006
c_3 ($\text{mg}\cdot\text{g}^{-1}$)	5.395	5.447	5.052	5.362
R^2	0.551	0.979	0.393	0.875

As depicted in Table 2, the pseudo-second-order kinetic model offers a superior fit for both phenol and catechol kinetic datasets, evident from the R^2 values exceeding 0.999. The calculated q_e values derived from the pseudo-second-order kinetic model for phenol and catechol adsorption onto 100C₁₂DAO-Bt and 150C₁₂DAO-Bt were in closer alignment with experimental q_e data, contrasting with values obtained from the pseudo-first-order kinetic model. This observation underscores a chemisorption process dictating the reaction dynamics. The presence of non-zero constants within the intraparticle diffusion model suggests that rate-limiting steps are influenced by a combination of factors beyond exclusive intraparticle diffusion. Moreover, the discernible decrement trends from the $K_{id,1}$ to $K_{id,3}$ demonstrate a gradual reduction in adsorption rate, attributed to the occupancy of active sites.

Upon comparison with previously explored organo-clays (as presented in Table 3), it becomes evident that the synthesis temperature for C₁₂DAO-Bt stands lower than that of several counterparts [16,48]. Additionally, the adsorption capacities of C₁₂DAO-Bt, derived from the pseudo-second-order kinetic model, for phenol removal either match or even surpass those of certain organo-clays [49]. It is pertinent to note the scarcity of empirical evidence concerning catechol removal from wastewater using organo-modified clays.

Table 3. The pseudo-second-order kinetic model-based adsorption capacity of C₁₂DAO-Bt for phenol and catechol in comparison to other organo-modified clays.

Adsorbates	Clay-Based Adsorbents	Preparation	Adsorption Capacity ($\text{mg}\cdot\text{g}^{-1}$)	Experimental Conditions	References
Phenol	BHM	25 °C, 3 h	7.97	$C_0 = 60 \text{ mg}\cdot\text{L}^{-1}$; $T = 25 \text{ }^\circ\text{C}$; $\text{pH} = 6.5$	[49]
	BPM	25 °C, 3 h	3.20		
	KHM	25 °C, 3 h	1.82		
	KPM	25 °C, 3 h	0.59		
	OMB	70 °C, 2 h	7.14	$C_0 = 100 \text{ mg}\cdot\text{L}^{-1}$; $T = 25 \text{ }^\circ\text{C}$; $\text{pH} = 10$.	[16]
	FTMA-MT	60 °C, 1 h	18.70		
	BHHP-MT	60 °C, 3 h	13.52	$C_0 = 120 \text{ mg}\cdot\text{L}^{-1}$; $T = 25 \text{ }^\circ\text{C}$; $\text{pH} = 7$.	[24]
	BOHP-MT	60 °C, 3 h	6.30		
	C12DAO-Bt	25 °C, 3 h	5.72	$C_0 = 200 \text{ mg}\cdot\text{L}^{-1}$; $T = 25 \text{ }^\circ\text{C}$; $\text{pH} = 6$.	[48]
				$C_0 = 120 \text{ mg}\cdot\text{L}^{-1}$; $T = 25 \text{ }^\circ\text{C}$; $\text{pH} = 6\text{--}6.5$.	This study

Table 3. Cont.

Adsorbates	Clay-Based Adsorbents	Preparation	Adsorption Capacity (mg·g ⁻¹)	Experimental Conditions	References
Catechol	BHHP-MT	60 °C, 3 h	32.04	C ₀ = 200 mg·L ⁻¹ ; T = 25 °C; pH = 6.	[48]
	BOHP-MT	60 °C, 3 h	19.51		
	C12DAO-Bt	25 °C, 3 h	5.55	C ₀ = 120 mg·L ⁻¹ ; T = 25 °C; H = 6~6.5.	This study

BHM, hexadecyltrimethylammonium-modified bentonite; BPM, phenyl trimethylammonium-modified bentonite; KHM, hexadecyltrimethylammonium-modified kaolinite; KPM, phenyl trimethylammonium-modified kaolinite; OMB, cetyltrimethylammonium bromide-modified bentonite; FTMA-MT, trimethylammonium bromide-modified montmorillonite; BHHP-MT, 1,3-bis(hexadecyldimethylammonio)-2-hydroxypropane dichloride-modified montmorillonite; BOHP, 1,3-bis(octyldimethylammonio)-2-hydroxypropane dichloride-modified montmorillonite.

3.4.3. Effect of Solution pH

The role of solution pH as a critical factor affecting adsorption ability has been well established, stemming from the intricate interplay between the surface charge of the adsorbents [39] and the species involved and the ionization extent of phenolic solutes [48]. This study investigates the impact of solution pH on the adsorption capacity of C₁₂DAO-Bt for phenol and catechol. A series of ten pH gradients ranging from 2 to 10, with intervals of 1, were employed for the batch adsorption of phenol and catechol, and the results are illustrated in Figure 6a,b. As observed, there are analogous trends in the fluctuations of adsorption capacities for phenolic compounds onto C₁₂DAO-Bt across varying C₁₂DAO/bentonite mass ratios. A superior adsorption capacity was observed for phenol compared to catechol throughout the explored pH range. Upon increasing the pH from 2 to 4, both phenol and catechol adsorption capacities exhibit a gradual upsurge. A subsequent decline is noticeable as the pH reaches 5, which is in line with an earlier observation [24]. Remarkably, the adsorption efficiency for phenol and catechol peaks at pH 6. As the pH becomes more alkaline, the catechol experiences a swifter decline in comparison to phenol. These observations stem from the intricate interplay between the ionization extent of phenolic compounds [48] and the surface charge of the adsorbents within the solution [39].

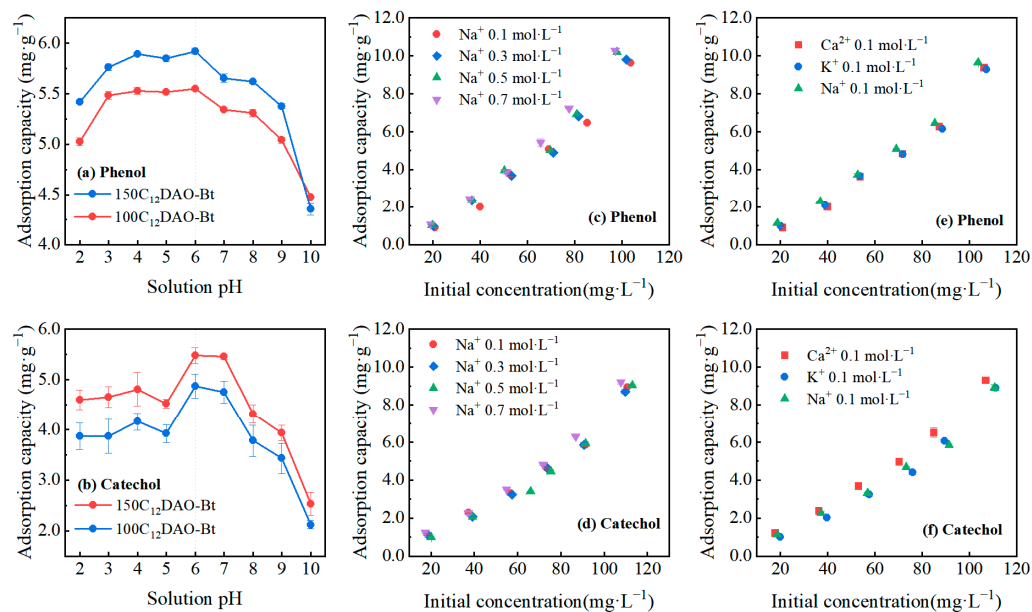


Figure 6. Effects of solution pH (a,b), cationic strength (c,d), and coexisting cation species (e,f) on adsorption for phenol and catechol by C₁₂DAO-Bt.

The acidity dissociation constants (*pK_a*) of phenol and catechol are recorded above 7, measuring 9.25 [50] and 9.95 [19], respectively, within aqueous solutions. Below their

respective pK_a values, these weak acid compounds predominantly exist in molecular forms, with partial dissociation into the negatively charged phenolate anions. The degree of ionization escalates with rising solution pH, thus leading to a higher presence of phenolate anions due to deprotonation in the solution [48]. Furthermore, the acid constant (pK_M) of C_{12} DAO micelles is estimated to be around 6.0 [37], indicative of the micelle's surface charge [28].

Under acidic and neutral conditions, the unchanged molecular structure of solutes can interface with the organic phase of C_{12} DAO-Bt attributed to van der Waals interaction, while the phenolate anions enable electrostatic interaction with positively charged adsorbents [46]. Conversely, electrostatic repulsion is attenuated between surfaces of negatively charged adsorbents and phenolate anions under alkaline conditions. In addition, the competition adsorption between the hydroxide ion (OH^-) and phenolic anions exerts a diminishing effect on adsorption capacity in alkaline solution. The observed optimal pH for phenol and catechol was 6.

3.4.4. Effect of Coexisting Ionic Strength and Species

Inorganic ions, Na^+ , K^+ , and Ca^{2+} , are ubiquitous in both industrial wastewaters and when naturally waterborne. As reported, ionic strength and ionic species exert a pivotal influence on the removal of phenolic compounds from wastewater [24,51]. To elucidate the intricate interplay between coexisting ionic strength and phenol adsorption, a comprehensive investigation was undertaken involving four distinct concentration gradients of NaCl (0.1, 0.3, 0.5, and 0.7 mol·L⁻¹). Furthermore, to thoroughly explore the impact of coexisting ionic species on the adsorption process, precise quantities of KCl, NaCl, and CaCl₂ were introduced into 20 mL solutions containing varied concentrations of phenols. This approach ensured a comparable ionic strength of 0.1 mol·L⁻¹ throughout the experimental regime. During the experiment, 100 C_{12} DAO-Bt was chosen as the test sample.

Figure 6c,d showcase an increasing adsorption of phenol and catechol by C_{12} DAO-Bt as the ionic strength elevates. This phenomenon is attributed to two aspects. Firstly, the introduction of NaCl into the solution induces a salting-out effect, reducing the solubility of phenols [52]. As a result, a larger quantity of phenols preferentially adheres to the C_{12} DAO-Bt surface. Secondly, the coexisting ions lead to limited dissociation of C_{12} DAO wormlike micelles [53], thereby amplifying their stability and promoting the adsorption of phenols by C_{12} DAO-Bt. In summary, heightened coexisting ionic strength in solution promotes the adsorption of phenol and catechol on C_{12} DAO-Bt.

Figure 6e,f reveal a more pronounced promotional effect of Na^+ on phenol adsorption when juxtaposed with K^+ and Ca^{2+} at an equivalent ionic strength. Ca^{2+} , possessing greater charges, inherently exhibits a heightened affinity for adsorption onto C_{12} DAO-Bt, leading to a reduction in phenol adsorption onto C_{12} DAO-Bt. Conversely, concerning catechol, a distinct promotional impact is evident with Ca^{2+} when contrasted with two other ionic species. This promotion can be attributed to the formation of a bridge between Ca^{2+} and two OH^- groups of catechol, facilitating its adhesion onto the adsorbent matrix.

3.5. Desorption Studies

3.5.1. Effect of C_{12} DAO/Bentonite Ratios on Desorption

This phase of experimentation focuses on investigating the impacts of varying C_{12} DAO/bentonite mass ratios on the desorption efficiency of absorbed phenol and catechol. In addition to the conditions outlined in Section 2.5, the experimental setup entails an initial adsorbate concentration set at 120 mg·L⁻¹ and a solution pH range between 8.5 and 10. For batch adsorption tests, we employed 100 C_{12} DAO-Bt and 150 C_{12} DAO-Bt as test samples, with raw-Bt serving as the control. The findings are presented in Figure 7a,b.

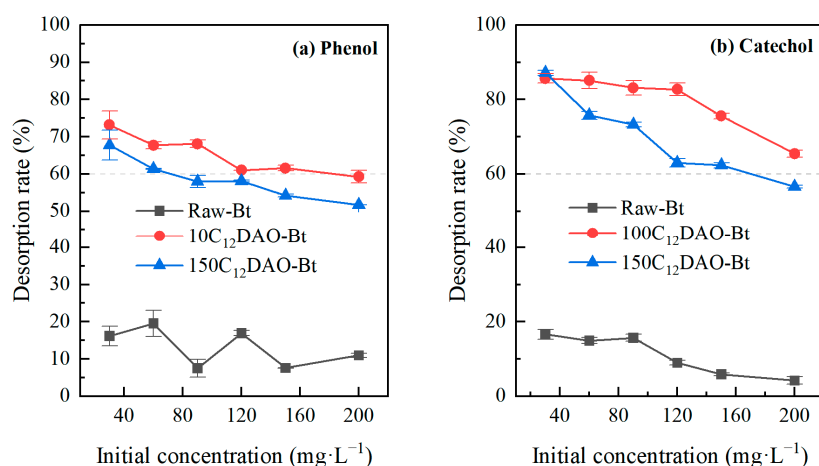


Figure 7. Effects of C₁₂DAO/bentonite ratios on desorption for phenol (a) and catechol (b).

The results clearly demonstrate enhanced desorption efficacies for both phenol and catechol in the context of C₁₂DAO/Bt as compared to raw-Bt. The desorption efficacies exhibit a declining trend as the initial adsorbate concentration increases. Overall, 100C₁₂DAO-Bt exhibited superior desorption efficacy than 150C₁₂DAO-Bt, which suggests an excessive abundance of surfactant concentration poses a hindrance to the desorption process. Within C₁₂DAO-Bt, the C₁₂DAO surfactant adheres extensively to the bentonite substrate through hydrophobic interactions originating from its carbon chains, which establishes a robust organic phase during the adsorption process. The pH modulation stimulates phase transformation in the surfactant and a morphological transition in the aggregate, facilitating the detachment of phenolic compounds from the substrate. However, the pH fluctuations within the system exert a minimal impact on the surfactant anchored onto the bentonite substrate through its elongated hydrophobic carbon chains, thus impeding the desorption process. As a result, the desorption efficacy of phenolic compounds on the highly loaded C₁₂DAO-Bt remains relatively low.

3.5.2. Effect of pH, Ionic Strength, and Species on Desorption

The C₁₂DAO micelles, known for their pH-sensitive behavior, undergo mutual transformations between spherical and wormlike aggregates dictated by changes in pH and ionic strength [54]. Within the context of the deposition experiment, the impact of solution pH, ionic strength, and ionic species on the desorption efficiency of phenol and catechol adsorption onto C₁₂DAO-Bt was examined. It was a comprehensive examination encompassing eleven pH levels spanning from 2 to 11, four distinct concentrations of Na⁺ ions (0.1, 0.3, 0.5, and 0.7 mol·L⁻¹), and three diverse ionic species (Na⁺, K⁺, and Ca²⁺) under an equivalent ionic strength of 0.1 mol·L⁻¹. The adsorbent of choice was 100C₁₂DAO-Bt.

As depicted in Figure 8a,b, the highest desorption efficacy was achieved for both phenol (80.24%) and catechol (66.54%) at pH 9, while the lowest values were observed at pH 6. These observations align with the alterations in adsorption capacity due to pH changes, as explained in Section 3.4.3. Under weakly acidic and neutral conditions, the wormlike micelles reach their optimal states, exhibiting enhanced viscoelastic properties. This is confirmed by the significantly higher viscosity at pH 6.4 compared to the observed values at pH 9.5 (Figure 1a). Under alkaline conditions, the transformation from wormlike to spherical micelles reduces solution viscosity and triggers the release of phenolic compounds trapped between the adsorbent layers.

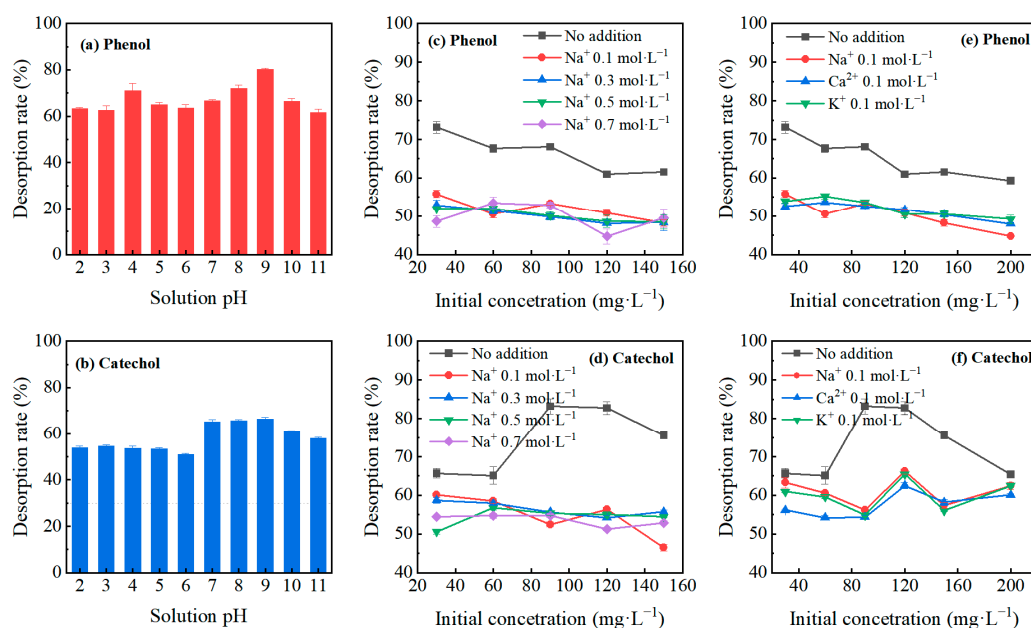


Figure 8. Effects of solution pH (a,b), cationic strength (b,d), and coexisting cation species (e,f) on desorption for phenol and catechol by 100C₁₂DAO-Bt.

As illustrated in Figure 8c,d, the presence of Na⁺ ions has a negative impact on the desorption of both phenol and catechol. However, the effect of ionic strength varies with the initial concentrations of solutes. This decrease in desorption efficacy can be attributed to the limited dissociation extent of C₁₂DAO wormlike micelles in the presence of cations, which favors the adsorption of phenolic compounds. Moving to Figure 9e,f, the largest reduction in desorption efficacy was observed in phenol/Na⁺ and catechol/Ca²⁺ coexisting systems, respectively, which is consistent with the aforementioned effect of ionic species on adsorption capacity.

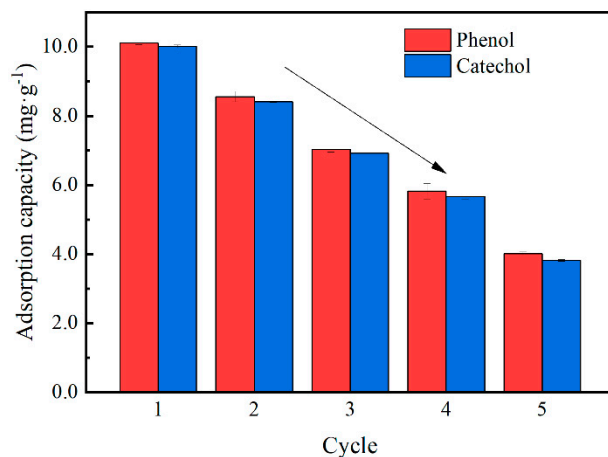


Figure 9. Adsorption capacity of 100C₁₂DAO-Bt for phenol and catechol.

3.6. Regeneration of C₁₂DAO-Bt through Acid–Base Regulation

To evaluate the regenerative ability of C₁₂DMAO-Bt, an extensive investigation was conducted using 150C₁₂DAO-Bt as the experimental target. The adsorbent underwent five consecutive cycles of acid–base regulation using HCl and NaOH, respectively. As revealed in Figure 9, the adsorption capacity of C₁₂DAO-Bt for phenol decreases from 10.11 mg·g⁻¹ to 4.01 mg·g⁻¹, while that of catechol drops from 10.01 mg·g⁻¹ to 3.82 mg·g⁻¹ over the five adsorption–desorption cycles. Notably, the approximately linear reductions signify a gradual decline in adsorption capacity over successive cycles. This phenomenon finds its rationale in the occupation of active sites on the adsorbent surface by phenol

and catechol during each desorption process. Simultaneously, the adsorbed pollutants encounter limitations in terms of complete liberation from the interlayer of C₁₂DAO-Bt. Herein, this interplay results in a discernible decrease in the subsequent adsorption cycles, leading to a reduced adsorption capacity of C₁₂DAO-Bt for both phenol and catechol compared to its initial effectiveness.

4. Conclusions

In this study, a novel type of C₁₂DAO-modified organo-bentonite was fabricated for the removal of phenol and catechol from wastewater. Functioning as a pH-sensitive surfactant, the solution viscosity changes reversibly with a pH-derived shape transition between spherical and wormlike micelles. The SEM images, XRD spectra, and FTIR spectrum depicted the physicochemical properties of adsorbents and confirmed the successful modification of C₁₂DAO-Bt. TG curves further exhibit the C₁₂DAO-Bt's excellent thermal stability. The kinetic data was well fitted by a pseudo-second-order kinetic model, indicating a chemisorption process. The highest adsorption capacity and desorption efficacy of phenol and catechol were observed at a pH range between 6 and 7 and from 8 to 9, respectively. A high C₁₂DAO/bentonite enhances the adsorption process but impedes the desorption process. The presence of elevating cationic strength within the examined range prompted the adsorption process but hindered the desorption efficacy. In the case of cationic species with equivalent ionic strength, Na⁺ exhibited a superior effect on the adsorption–desorption process of phenol, while Ca²⁺ showcased a greater impact on the adsorption–desorption process of catechol. Moreover, C₁₂DAO-Bt displayed a relatively high adsorption capacity and desorption efficacy, even after undergoing five consecutive adsorption–desorption cycles, which implies its excellent reusability for the removal of phenolic compounds from wastewater. The praiseworthy adsorption capacity and remarkable regenerative capabilities achieved through easy pH modulation offer promising prospects for addressing wastewater contamination by phenol and catechol. Nonetheless, it is judicious to recognize that achieving a more comprehensive understanding demands the incorporation of diverse variables and empirical investigations. Adopting this comprehensive approach will facilitate a more thorough assessment of its potential efficacy.

Author Contributions: All authors contributed to this work. Specifically, H.L. and Y.L. designed the experiments. J.L. conducted the experiments and performed the characterization. X.C. interpreted the data and worked out the manuscript. W.T., C.T. and S.T. advised on the conception and design of the study, as well as on the revision of the manuscripts. All authors have read and agreed to the published version of the manuscript.

Funding: This research was financially supported by the National Natural Science Foundation of China (41761072).

Institutional Review Board Statement: Not applicable.

Informed Consent Statement: Not applicable.

Data Availability Statement: All related data are included in the present paper or available upon request.

Conflicts of Interest: The authors declare no conflict of interest.

References

1. Anku, W.W.; Mamo, M.A.; Penny, P.G. Phenolic Compounds in Water: Sources, Reactivity, Toxicity and Treatment Methods. In *Phenolic Compounds*; Soto-Hernandez, M., Palma-Tenango, M., Garcia-Mateos, M.d.R., Eds.; IntechOpen: Rijeka, Croatia, 2017; Chapter 17. [[CrossRef](#)]
2. Kumar, A.; Kumar, S.; Kumar, S. Biodegradation Kinetics of Phenol and Catechol Using *Pseudomonas Putida* MTCC 1194. *Biochem. Eng. J.* **2005**, *22*, 151–159. [[CrossRef](#)]
3. Khan, N.; Anwer, A.H.; Ahmad, A.; Sabir, S.; Sevda, S.; Khan, M.Z. Investigation of Cnt/Ppy-Modified Carbon Paper Electrodes under Anaerobic and Aerobic Conditions for Phenol Bioremediation in Microbial Fuel Cells. *ACS Omega* **2020**, *5*, 471–480. [[CrossRef](#)] [[PubMed](#)]
4. Acosta, C.A.; Pasquali, C.E.L.; Paniagua, G.; Garcinuno, R.M.; Hernando, P.F. Evaluation of Total Phenol Pollution in Water of San Martin Canal from Santiago Del Estero, Argentina. *Environ. Pollut.* **2018**, *236*, 265–272. [[CrossRef](#)] [[PubMed](#)]

5. Panigrahy, N.; Priyadarshini, A.; Sahoo, M.M.; Verma, A.K.; Daverey, A.; Sahoo, N.K. A Comprehensive Review on Eco-Toxicity and Biodegradation of Phenolics: Recent Progress and Future Outlook. *Environ. Technol. Innov.* **2022**, *27*, 102423. [CrossRef]
6. USEPA. Emergency Planning and Community Right-to-Know Act (Epcra) Section 313 Chemical List for Reporting Year 2014. 2014. Available online: https://www.epa.gov/sites/default/files/2017-09/documents/chemical_list_for_reporting_year_2014.pdf (accessed on 1 January 2023).
7. Bibi, A.; Bibi, S.; Abu-Dieyeh, M.; Al-Ghouti, M.A. Towards Sustainable Physiochemical and Biological Techniques for the Remediation of Phenol from Wastewater: A Review on Current Applications and Removal Mechanisms. *J. Clean. Prod.* **2023**, *417*, 137810. [CrossRef]
8. Aravind, M.K.; Kappen, J.; Perumal, V.; John, S.A.; Balasubramaniam, A. Bioengineered Graphene Oxide Microcomposites Containing Metabolically Versatile *Paracoccus* Sp. Mku1 for Enhanced Catechol Degradation. *ACS Omega* **2020**, *5*, 16752–16761. [CrossRef]
9. Linh, N.L.M.; Duong, T.; Duc, H.V.; Thu, N.T.A.; Lieu, P.K.; Hung, N.V.; Hoa, L.T.; Khieu, D.Q. Phenol Red Adsorption from Aqueous Solution on the Modified Bentonite. *J. Chem.* **2020**, *2020*, 1504805. [CrossRef]
10. Yao, T.; Li, H.M.; Ren, Y.H.; Feng, M.L.; Hu, Y.C.; Yan, H.L.; Peng, L. Extraction and Recovery of Phenolic Compounds from Aqueous Solution by Thermo-Separating Magnetic Ionic Liquid Aqueous Two-Phase System. *Sep. Purif. Technol.* **2022**, *282*, 120034. [CrossRef]
11. Ramos, R.L.; Moreira, V.R.; Lebron, Y.A.R.; Santos, L.V.S.; Amaral, M.C.S. Fouling in the Membrane Distillation Treating Superficial Water with Phenolic Compounds. *Chem. Eng. J.* **2022**, *437*, 135325. [CrossRef]
12. Zhou, S.; Guo, J.; Zou, Y.; Wang, L.; Kaw, H.Y.; Quinto, M.; Meng, L.Y.; Dong, M. Fast Removal of Phenolic Compounds from Water Using Hierarchical Porous Carbon Nanofibers Membrane. *J. Chromatogr. A* **2022**, *1685*, 463624. [CrossRef]
13. Men, X.P.; Guo, Q.X.; Meng, B.; Ren, S.Y.; Shen, B.J. Adsorption of Bisphenol a in Aqueous Solution by Composite Bentonite with Organic Moity. *Microporous Mesoporous Mater.* **2020**, *308*, 110450. [CrossRef]
14. Awad, A.M.; Shaikh, S.M.R.; Jalab, R.; Gulied, M.H.; Nasser, M.S.; Benamor, A.; Adham, S. Adsorption of Organic Pollutants by Natural and Modified Clays: A Comprehensive Review. *Sep. Purif. Technol.* **2019**, *228*, 115719. [CrossRef]
15. Al-Asheh, S.; Banat, F.; Abu-Aitah, L. Adsorption of Phenol Using Different Types of Activated Bentonites. *Sep. Purif. Technol.* **2003**, *33*, 1–10. [CrossRef]
16. He, H.J.; Xu, E.R.; Qiu, Z.H.; Wu, T.; Wang, S.F.; Lu, Y.H.; Chen, G.N. Phenol Adsorption Mechanism of Organically Modified Bentonite and Its Microstructural Changes. *Sustainability* **2022**, *14*, 1318. [CrossRef]
17. Wang, G.F.; Wang, X.L.; Zhang, S.; Ma, S.J.; Wang, Y.W.; Qiu, J. Adsorption of Heavy Metal and Organic Pollutant by Organo-Montmorillonites in Binary-Component System. *J. Porous Mater.* **2020**, *27*, 1515–1522. [CrossRef]
18. Orucoglu, E.; Schroeder, P.A. Investigating the Expanding Behavior and Thermal Stability of Hdpv Modified Organo-Bentonite by X-ray Diffraction Technique. *Appl. Clay Sci.* **2016**, *132–133*, 90–95. [CrossRef]
19. Hu, X.L.; Meng, Z.F.; Cao, X.W.; Liu, Z.; Wu, Z.B.; Sun, H.L.; Sun, X.; Li, W.B. Effect of Double Carbon Chains on Enhanced Removal of Phenol from Wastewater by Amphoteric-Gemini Complex-Modified Bentonite. *Environ. Pollut.* **2023**, *320*, 121088. [CrossRef]
20. Szabó, E.; Pap, Z.; Simon, G.; Dombi, A.; Baia, L.; Hernádi, K. New Insights on the Simultaneous Removal by Adsorption on Organoclays of Humic Acid and Phenol. *Water* **2015**, *8*, 21. [CrossRef]
21. Khodabakhshloo, N.; Biswas, B.; Moore, F.; Du, J.H.; Naidu, R. Organically Functionalized Bentonite for the Removal of Perfluorooctane Sulfonate, Phenanthrene and Copper Mixtures from Wastewater. *Appl. Clay Sci.* **2021**, *200*, 105883. [CrossRef]
22. Zhai, C.; Azhar, U.; Yue, W.; Dou, Y.; Zhang, L.; Yang, X.; Zhang, Y.; Xu, P.; Zong, C.; Zhang, S. Preparation and Insights of Smart Foams with Phototunable Foamability Based on Azobenzene-Containing Surfactants. *Langmuir* **2020**, *36*, 15423–15429. [CrossRef]
23. Pei, X.; Zhang, S.; Zhang, W.; Liu, P.; Song, B.; Jiang, J.; Cui, Z.; Binks, B.P. Behavior of Smart Surfactants in Stabilizing Ph-Responsive Emulsions. *Angew. Chem. Int. Ed. Engl.* **2021**, *60*, 5235–5239. [CrossRef] [PubMed]
24. Li, Y.J.; Hu, X.J.; Liu, X.L.; Zhang, Y.C.; Zhao, Q.; Ning, P.; Tian, S.L. Adsorption Behavior of Phenol by Reversible Surfactant-Modified Montmorillonite: Mechanism, Thermodynamics, and Regeneration. *Chem. Eng. J.* **2018**, *334*, 1214–1221. [CrossRef]
25. Liu, Y.X.; Jessop, P.G.; Cunningham, M.; Eckert, C.A.; Liotta, C.L. Switchable Surfactants. *Science* **2006**, *313*, 958–960. [CrossRef] [PubMed]
26. Kawasaki, H.; Souda, M.; Tanaka, S.; Nemoto, N.; Karlsson, G.; Almgren, M.; Maeda, H. Reversible Vesicle Formation by Changing pH. *J. Phys. Chem. B* **2002**, *106*, 1524–1527. [CrossRef]
27. Huibers, P.D.T. Quantum-Chemical Calculations of the Charge Distribution in Ionic Surfactants. *Langmuir* **1999**, *15*, 7546–7550. [CrossRef]
28. Scermino, L.; Fabozzi, A.; De Tommaso, G.; Valente, A.J.M.; Iuliano, M.; Paduano, L.; D'Errico, G. pH-Responsive Micellization of an Amine Oxide Surfactant with Branched Hydrophobic Tail. *J. Mol. Liq.* **2020**, *316*, 113799. [CrossRef]
29. Hoffmann, H. Fascinating Phenomena in Surfactant Chemistry. *Adv. Mater.* **1994**, *6*, 116–129. [CrossRef]
30. Hoffmann, H. Viscoelastic Surfactant Solutions. In *Structure and Flow in Surfactant Solutions*; 2-31; American Chemical Society: Washington, DC, USA, 1994.
31. Zhou, J.; Ranjith, P.G. Self-Assembly and Viscosity Changes of Binary Surfactant Solutions: A Molecular Dynamics Study. *J. Colloid Interface Sci.* **2021**, *585*, 250–257. [CrossRef]
32. Jia, H.; He, J.; Wang, Q.X.; Xu, Y.B.; Zhang, L.Y.; Jia, H.D.; Song, L.; Wang, Y.; Xie, Q.; Wu, H.Y. Investigation on Novel Redox-Responsive Ferrocenyl Surfactants with Reversible Interfacial Behavior and Their Recycling Application for Enhanced Oil Recovery. *Colloids Surf. A Physicochem. Eng. Asp.* **2022**, *653*, 129971. [CrossRef]

33. Zhu, J.; Qing, Y.; Wang, T.; Zhu, R.; Wei, J.; Tao, Q.; Yuan, P.; He, H. Preparation and Characterization of Zwitterionic Surfactant-Modified Montmorillonites. *J Colloid Interface Sci.* **2011**, *360*, 386–392. [[CrossRef](#)]
34. Hu, X.J.; Tian, S.L.; Zhan, S.J.; Zhu, J.X. Adsorption of Switchable Surfactant Mixed with Common Nonionic Surfactant on Montmorillonite: Mechanisms and Arrangement Models. *Appl. Clay Sci.* **2017**, *146*, 140–146. [[CrossRef](#)]
35. Liu, C.M.; Wu, P.X.; Zhu, Y.J.; Tran, L. Simultaneous Adsorption of Cd²⁺ and BPA on Amphoteric Surfactant Activated Montmorillonite. *Chemosphere* **2016**, *144*, 1026–1032. [[CrossRef](#)] [[PubMed](#)]
36. Guo, X.B.; Wu, Z.J.; Wang, Z.L.; Lin, F.F.; Li, P.H.; Liu, J.X. Preparation of Chitosan-Modified Bentonite and Its Adsorption Performance on Tetracycline. *ACS Omega* **2023**, *8*, 19455–19463. [[CrossRef](#)] [[PubMed](#)]
37. Maeda, H. A Thermodynamic Analysis of the Hydrogen Ion Titration of Micelles. *J. Colloid Interface Sci.* **2003**, *263*, 277–287. [[CrossRef](#)] [[PubMed](#)]
38. Pawar, R.R.; Lalhmunsiam; Ingole, P.G.; Lee, S.M. Use of Activated Bentonite-Alginate Composite Beads for Efficient Removal of Toxic Cu²⁺ and Pb²⁺ Ions from Aquatic Environment. *Int. J. Biol. Macromol.* **2020**, *164*, 3145–3154. [[CrossRef](#)]
39. Yang, J.B.; Huang, B.; Lin, M.Z. Adsorption of Hexavalent Chromium from Aqueous Solution by a Chitosan/Bentonite Composite: Isotherm, Kinetics, and Thermodynamics Studies. *J. Chem. Eng. Data* **2020**, *65*, 2751–2763. [[CrossRef](#)]
40. Zhu, J.X.; Zhang, P.; Qing, Y.H.; Wen, K.; Su, X.L.; Ma, L.Y.; Wei, J.; Liu, H.; He, H.; Xi, Y.F. Novel Intercalation Mechanism of Zwitterionic Surfactant Modified Montmorillonites. *Appl. Clay Sci.* **2017**, *141*, 265–271. [[CrossRef](#)]
41. Chen, B.L.; Zhu, L.Z.; Zhu, J.X.; Xing, B.S. Configurations of the Bentonite-Sorbed Myristylpyridinium Cation and Their Influences on the Uptake of Organic Compounds. *Environ. Sci. Technol.* **2005**, *39*, 6093–6100. [[CrossRef](#)]
42. Fu, X.W.; Kong, W.B.; Zhang, Y.Y.; Jiang, L.; Wang, J.L.; Lei, J.X. Novel Solid–Solid Phase Change Materials with Biodegradable Trihydroxy Surfactants for Thermal Energy Storage. *RSC Adv.* **2015**, *5*, 68881–68889. [[CrossRef](#)]
43. Atykhan, N.; Revin, V.; Shutova, V. Raman and FT-IR Spectroscopy Investigation the Cellulose Structural Differences from Bacteria *Gluconacetobacter SuCrofermentans* During the Different Regimes of Cultivation on a Molasses Media. *AMB Express* **2020**, *10*, 84. [[CrossRef](#)]
44. Kalburcu, T.; Tabak, A.; Ozturk, N.; Tuzmen, N.; Akgol, S.; Caglar, B.; Denizli, A. Adsorption of Lysozyme from Aqueous Solutions by a Novel Bentonite–Tryptophane (Bent–Trp) Microcomposite Affinity Sorbent. *J. Mol. Struct.* **2015**, *1083*, 156–162. [[CrossRef](#)]
45. Wang, G.F.; Wang, S.; Sun, Z.M.; Zheng, S.L.; Xi, Y.F. Structures of Nonionic Surfactant Modified Montmorillonites and Their Enhanced Adsorption Capacities Towards a Cationic Organic Dye. *Appl. Clay Sci.* **2017**, *148*, 1–10. [[CrossRef](#)]
46. Shakir, K.; Ghoneimy, H.F.; Elkafrawy, A.F.; Beheir Sh, G.; Refaat, M. Removal of Catechol from Aqueous Solutions by Adsorption onto Organophilic-Bentonite. *J. Hazard. Mater.* **2008**, *150*, 765–773. [[CrossRef](#)] [[PubMed](#)]
47. Chen, D.M.; Chen, J.; Luan, X.L.; Ji, H.P.; Xia, Z.G. Characterization of Anion–Cationic Surfactants Modified Montmorillonite and Its Application for the Removal of Methyl Orange. *Chem. Eng. J.* **2011**, *171*, 1150–1158. [[CrossRef](#)]
48. Liu, Y.N.; Gao, M.L.; Gu, Z.; Luo, Z.X.; Ye, Y.G.; Lu, L.F. Comparison between the Removal of Phenol and Catechol by Modified Montmorillonite with Two Novel Hydroxyl-Containing Gemini Surfactants. *J. Hazard. Mater.* **2014**, *267*, 71–80. [[CrossRef](#)]
49. Alkaram, U.F.; Mukhlis, A.A.; Al-Dujaili, A.H. The Removal of Phenol from Aqueous Solutions by Adsorption Using Surfactant-Modified Bentonite and Kaolinite. *J. Hazard. Mater.* **2009**, *169*, 324–332. [[CrossRef](#)]
50. Suresh, S.; Srivastava, V.C.; Mishra, I.M. Adsorption of Catechol, Resorcinol, Hydroquinone, and Their Derivatives: A Review. *Int. J. Energy Environ. Eng.* **2012**, *3*, 32. [[CrossRef](#)]
51. Jiang, L.; Yu, Z.J.; Liu, Y.J.; Xian, M.; Xu, C. Mechanisms Associated with the Separation of Phenols from Complex Coexisting Systems. *J. Environ. Chem. Eng.* **2022**, *10*, 107889. [[CrossRef](#)]
52. Khalifa, A.; Mellouk, S.; Marouf-Khelifa, K.; Khelifa, A. Removal of Catechol from Water by Modified Dolomite: Performance, Spectroscopy, and Mechanism. *Water Sci. Technol.* **2018**, *77*, 1920–1930. [[CrossRef](#)]
53. Maeda, H.; Kakehashi, R. Effects of Protonation on the Thermodynamic Properties of Alkyl Dimethylamine Oxides. *Adv. Colloid Interface Sci.* **2000**, *88*, 275–293. [[CrossRef](#)]
54. Majhi, P.R.; Dubin, P.L.; Feng, X.H.; Guo, X.H.; Leermakers, F.A.M.; Tribet, C. Coexistence of Spheres and Rods in Micellar Solution of Dodecyldimethylamine Oxide. *J. Phys. Chem. B* **2004**, *108*, 5980–5988. [[CrossRef](#)]

Disclaimer/Publisher’s Note: The statements, opinions and data contained in all publications are solely those of the individual author(s) and contributor(s) and not of MDPI and/or the editor(s). MDPI and/or the editor(s) disclaim responsibility for any injury to people or property resulting from any ideas, methods, instructions or products referred to in the content.